Check for updates

Polymer Engineering & Science

WILEY | spe INSPIRING PLASTICS PROFESSIONALS

RESEARCH ARTICLE OPEN ACCESS

Investigation of a Polyamide 6 (PA6) and Polybutylene Succinate (PBS) Blend as Candidate Matrix for Self-Healing Application

Laura Simonini[1,2] | Riccardo Ramundo[1,2] | Daniele Rigotti[1,2] | Alessandro Sorze[1,2] | Alessandro Pegoretti[1,2] | Andrea Dorigato[1,2]

[1]Department of Industrial Engineering, University of Trento, Trento, Italy | [2]National Interuniversity Consortium of Materials Science and Technology (INSTM), Florence, Italy

Correspondence: Laura Simonini (laura.simonini@unitn.it)

Received: 9 July 2026 | **Revised:** 2 September 2026 | **Accepted:** 4 September 2026

Keywords: blends | composites | fracture toughness | PA6 | PBS | self-healing

ABSTRACT

In this work, polyamide 6/polybutylene succinate (PA6/PBS) blends, containing 20% to 50%vol of PBS, were melt compounded and hot pressed. Their rheological, morphological, thermo-mechanical, and fracture toughness properties were analyzed. Rheological analysis demonstrated that lower PBS contents increased the storage and loss moduli of PA6, maintaining good processability. FT-IR and FESEM observations showed the formation of PBS domains dispersed within the PA6 matrix. Mechanical tests revealed a progressive decrease in tensile modulus and strength with PBS content. However, blends containing 20%–30%vol PBS retained suitable levels of stiffness and strength compared to neat PA6. Particularly, the formulation containing 30%vol of PBS was selected as a candidate composition for self-healing assessment. The repair efficiency was quantified as the recovery of the fracture toughness after thermal treatment at 140°C. A recovery of 40% of the original dynamic fracture toughness under impact conditions was obtained, attributed to a smooth fracture surface generated at high strain rate, which could have promoted possible flow of the molten PBS across the crack interface during the healing process. Thus, the selected blend developed within this investigation could be considered in the future for the preparation of multifunctional composite laminates with thermal healing capability.

1 | Introduction

Polymer composites are widely used in structural applications due to their high strength-to-weight ratio, corrosion resistance, and design versatility. They are being used in transportation [1], aerospace [2], construction [3, 4] and energy sectors [5, 6], where material must deliver both mechanical performance and lightness. However, their main drawback lies in the vulnerability to microdamage, such as cracks and voids in the matrix [7, 8], fiber/matrix interfacial debonding [9–15] or interlaminar fracture [16, 17], which cause a progressive deterioration of the mechanical integrity of the structure. Considering that repair and maintenance operations are often complex and costly, in recent years there has been significant interest in the development of polymer composites that can repair damage autonomously, known as self-healing composites, as a strategy to increase reliability, reduce maintenance and extend service lifetime [18]. These materials possess the ability to recover their structural integrity after damage by partially mimicking the biological self-repair mechanisms observed in nature [19].

Self-healing materials are generally divided into extrinsic and intrinsic categories. Extrinsic systems use healing agents that are encapsulated in microcapsules [20] or vascular networks

This is an open access article under the terms of the Creative Commons Attribution License, which permits use, distribution and reproduction in any medium, provided the original work is properly cited.

© 2026 The Author(s). *Polymer Engineering & Science* published by Wiley Periodicals LLC on behalf of Society of Plastics Engineers.

Highlights

- Blends of PA6 and 20%–50%vol PBS prepared by melt compounding and hot pressing.
- PBS dispersed as micrometric domains embedded in the PA6 matrix.
- 30%vol PBS exhibited 40% fracture toughness recovery under impact loading.

[21], which are released upon fracture to fill the damaged area. Although this method can successfully recover the mechanical properties of a damaged material, its healing capability is limited to a single cycle because the encapsulated repair agent is consumed during the restoration process. In addition, the presence of microcapsules can negatively influence the material structure by introducing stress concentration sites that may promote defects within the matrix. Their incorporation can also create processing challenges, particularly by increasing the viscosity of the matrix during the molten or liquid processing stages [22]. Conversely, intrinsic self-healing mechanisms rely on reversible molecular interactions within the matrix, such as reversible hydrogen bonds, supramolecular associations, or thermally activated chain mobility [23–26]. These systems can heal repeatedly under mild external stimuli such as heat, making them highly attractive for high-performance thermoplastics. Among intrinsics, one of the most effective strategies involves embedding a thermoplastic polymer within the matrix as a healing component. Upon exposure to temperatures above the melting or softening point of this polymer, the healing phase becomes mobile, allowing it to flow into cracks and damaged regions. Since the thermoplastic agent is physically integrated into the polymer matrix, whether thermosetting or thermoplastic, its subsequent melting and redistribution facilitate crack filling and contribute to the restoration of the material's mechanical performance. For instance, Savioli et al. [27] blended poly(-lactic acid) (PLA) with increasing amounts of poly(butylene adipate-co-terephthalate) (PBAT) up to 30% by weight, obtaining blends with immiscible morphology constituted by PBAT domains dispersed within the PLA matrix. The addition of PBAT reduced the PLA's brittleness and imparted self-healing ability, restoring up to 64% of the original fracture toughness upon thermal mending at 140°C. Peñas-Caballero et al. [28] investigated an epoxy resin blended with poly(ethylene-co-methacrylic acid) (EMAA), resulting in immiscible thermoplastic domains within the thermosetting matrix, achieving up to 45% recovery of tensile strength upon thermal mending at 150°C.

Alongside the development of self-healing materials, the market for thermoplastic composites is growing rapidly, driven by the demand for lighter, durable, and recyclable structural solutions. The global thermoplastic composites market has been valued at $32.2 billion in 2021 and is expected to reach $62.6 billion by 2030, with a compound annual growth rate (CAGR) of 7.8% from 2022 to 2030 [29]. The growth of this market is therefore stimulating interest in the design and optimization of multifunctional thermoplastic composite matrices, with particular attention to polyamide-based systems [30].

Polyamide 6 (PA6) is a thermoplastic polymer synthesized through the ring-opening polymerization of caprolactam [31]. It is widely used in structural applications such as automotive components and fiber-reinforced composites [30, 32, 33]. However, despite its high stiffness and strength, PA6 can exhibit limited resistance to crack initiation and propagation under mechanical loading, which may compromise the durability of structural components [34]. To overcome this problem, blending PA6 with a tougher polymer that can also act as a self-healing phase represents a promising route toward multifunctional matrices with optimized mechanical properties [35]. In this context, Perin et al. [36] developed blends of PA6 with a cyclic olefin copolymer (COC) as healing agent. In their initial study, they examined PA6/COC blends compatibilized with ethylene glycidyl methacrylate (E-GMA) and showed that, upon thermal activation, COC effectively flowed and filled microcracks, enabling partial restoration of the original fracture toughness (68% under impact conditions). In another study of the same group [37], they adjusted the E-GMA content and healing temperature in PA6/COC blends, finding that a higher compatibilizer amount (i.e., 5 wt%) improved the interfacial adhesion and the self-healing efficiency of the blends. However, in all these systems the inherent brittleness of COC limited the fracture toughness of the resulting materials.

In order to overcome these limitations, the present work aims at designing a PA6-based blend in which the second phase is not only capable of self-healing but it is also ductile, in order to simultaneously heal and toughen the matrix. For instance, poly(butylene succinate) (PBS) is a biodegradable aliphatic polyester known for its elevated ductility and excellent thermal processability [38]. It exhibits a relatively low melting point (115°C–120°C) that makes it particularly promising in intrinsic self-healing applications, as it can melt and flow into cracks when heated to moderate temperatures (i.e., 120°C–150°C). Therefore, the combination of the thermo-mechanical performance of PA6 with the ductility of PBS at the molten state creates opportunities for designing novel self-healing thermoplastic matrices for structural applications. To the best of the authors' knowledge, there are no reported studies focused on the investigation of the thermo-mechanical and self-healing features of PA6/PBS blends. Therefore, the objective of this research was to identify a candidate PA6/PBS blend composition to combine satisfactory structural performance and self-healing capability. In order to achieve this goal, the developed blends were analyzed through rheological, morphological and thermo-mechanical characterization. Based on this preliminary screening, a candidate composition was selected for detailed fracture toughness and self-healing characterization under both quasi-static and impact loading conditions. The selection was based on the identification of a PBS content providing a suitable combination of retained thermo-mechanical performance while incorporating a sufficiently high fraction of the healing phase. The self-repairing performance was assessed by quantifying the recovery of fracture toughness after a thermal healing cycle carried out at 140°C, a temperature exceeding the melting point of PBS. This material could be then utilized in the future as a self-healing matrix in multifunctional composite laminates, in combination with glass and carbon fibers.

15482634, 2026, 11, Downloaded from https://4spepublications.onlinelibrary.wiley.com/doi/10.1002/pen.70863 by Alessandro Pegoretti - Universita Di Trento , Wiley Online Library on [01/11/2025]. See the Terms and Conditions (https://onlinelibrary.wiley.com/terms-and-conditions) on Wiley Online Library for rules of use; OA articles are governed by the applicable Creative Commons License

2 | Experimental Part

2.1 | Materials

The thermoplastic matrix was a Radilon S BF 990 GY polyamide 6 (PA6), provided in the form of granules by Radici Group (Bergamo, Italy), with a density of 1.14 g/cm^3, average molecular weight (M_w) of 60,000 g/mol, melt flow index (MFI) of 20 g/10 min (275°C, 5 kg) and a melting temperature of 220°C. The self-healing agent was a BioPBS FD 92 PM poly(butylene succinate) (PBS), supplied by PTT MCC Biochem (Chatuchak, Thailand) in the form of granules, with a density of 1.24 g/cm^3, M_w of 100,000 g/mol, MFI of 4 g/10 min (190°C, 2.16 kg) and a melting temperature of 110°C.

2.2 | Sample Preparation

Before processing, PA6 and PBS pellets were dried under vacuum in a laboratory oven to remove residual moisture, using temperatures of 80°C and 65°C, respectively, for 4 days. After drying, the required amounts of the two polymers were weighed according to the desired compositions and premixed manually before melt blending. Compounding was carried out in a Thermo Haake Rheomix 600 internal mixer (Thermo Fisher Scientific Inc., Waltham, MA, USA) equipped with counter-rotating rotors. The blending process was performed at 230°C for 5 min, with a rotor speed of 60 rpm, ensuring complete melting and homogeneous dispersion of the PBS phase within the PA6 matrix. The thermal stability of PA6 and PBS was assessed using thermogravimetric analysis (TGA), which revealed that both polymers exhibited an onset of thermal degradation above 300°C (see Figure S1). The compounded materials were subsequently shaped by compression molding using a Carver hot-plate press (Carverpress Inc., Wabash, IN, USA). The blends were molded at 220°C for 7 min under a pressure of 3.4 MPa, producing square plates with dimensions of 120 × 120 mm^2 and a thickness of 2 mm. Additional plates having the same in-plane dimensions but a thickness of 5 mm were manufactured for the preparation of Single Edge Notched Bending (SENB) specimens used in fracture toughness and self-healing tests. The compositions investigated in this study are listed in Table 1, together with the corresponding volume and weight fractions of each constituent.

TABLE 1 | List of the prepared blends.

Samples	PA6 (%vol)	PBS (%vol)	PA6 (%wt)	PBS (%wt)
PA6	100	—	100	—
PA6_20P	80	20	79	21
PA6_30P	70	30	68	32
PA6_40P	60	40	58	42
PA6_50P	50	50	48	52
PBS	—	100	—	100

2.3 | Experimental Techniques

2.3.1 | Rheological Properties

The viscoelastic behavior of the blends in the molten state was investigated using a Discovery Hybrid Rheometer (DHR-2, TA Instruments, New Castle, DE, USA) equipped with parallel plates (25 mm diameter). Measurements were carried out at 230°C using a 1 mm gap between the plates. Oscillatory frequency sweep tests were performed within the linear viscoelastic region by applying a strain amplitude of 1% over an angular frequency range from 0.1 to 100 rad s^{-1}. The storage modulus (G'), loss modulus (G''), and magnitude of complex viscosity (η^*) were recorded for each formulation. One specimen was analyzed for each composition.

2.3.2 | Chemical and Microstructural Properties

The chemical structure of the prepared blends was examined by Fourier-transform infrared spectroscopy (FTIR) using a PerkinElmer Spectrum One spectrometer operating in attenuated total reflectance (ATR) mode. Spectra were collected between 4000 and 650 cm^{-1} with a spectral resolution of 4 cm^{-1}, averaging four consecutive scans for each sample. One specimen was analyzed for every formulation.

The morphology of the blends was investigated by field-emission scanning electron microscopy (FESEM) using a Zeiss Supra 40 microscope (Carl Zeiss AG, Oberkochen, Germany). Cryogenically fractured specimens, both before and after the healing treatment, were sputter-coated with an approximately 5 nm thick Pt/Pd (80:20) conductive layer and observed at an accelerating voltage of 3.5 kV. The dimensions of the dispersed PBS domains were quantified through image analysis using ImageJ (version 1.53a).

2.3.3 | Thermal Properties

The thermal behavior of the blends was evaluated by differential scanning calorimetry (DSC) using a Mettler DSC30 calorimeter (Mettler Toledo Inc., Columbus, OH, USA). Measurements were carried out under a nitrogen atmosphere (100 mL min^{-1}) between −50°C and 250°C, employing heating and cooling rates of 10°C min^{-1}. Each specimen underwent a first heating cycle, a controlled cooling stage, and a second heating cycle. Glass transition temperature (T_g), crystallization temperature (T_c), melting temperature (T_m), and melting enthalpy (ΔH_m) of both polymer phases were determined. Equation (1) was used to calculate the degree of crystallinity of PA6 and PBS phases (χ) in the blends,

$$X(\%) = \frac{\Delta \mathrm{H_m}}{\Delta \mathrm{H_m^0} \times \mathrm{w}} \times 100 \quad (1)$$

where ΔH_m is the measured melting enthalpy of PA6 (or PBS) and ΔH_m^0 is the melting enthalpy of the 100% crystalline PA6 (230.0 J/g [39]) or PBS (110.3 J/g [40]), while w is the weight fraction of PA6 (or PBS) in the blends. One specimen was tested for each composition.

15482634, 2026, 11, Downloaded from https://4spepublications.onlinelibrary.wiley.com/doi/10.1002/pen.70863 by Alessandro Pegoretti - Universita Di Trento , Wiley Online Library on [01/11/2025]. See the Terms and Conditions (https://onlinelibrary.wiley.com/terms-and-conditions) on Wiley Online Library for rules of use; OA articles are governed by the applicable Creative Commons License

2.3.4 | Mechanical Properties

The tensile response of the blends was assessed at room temperature using an Instron 5969 universal testing machine equipped with a 10 kN load cell. Type 1BA specimens were tested following ISO 527. Elastic modulus measurements were performed at a crosshead speed of 0.25 mm/min, limiting the maximum strain to 1%. Axial deformation was monitored with an Instron 2620–601 extensometer (gauge length: 12.5 mm), and the modulus was calculated as the secant slope between 0.05% and 0.25% strain, according to the standard. Ultimate tensile strength (UTS) and elongation at break were determined at a crosshead speed of 5 mm/min without the extensometer. At least five specimens were tested for each formulation.

The Vicat softening temperature (VST) was measured according to ASTM D1525 using an ATS Faar MP/3 HDT-Vicat tester. Rectangular specimens ($10\times10\times5\,mm^3$) were tested under a 50 N load while heating at 120°C/h. Three measurements were performed for each composition.

Fracture toughness was evaluated on Single Edge Notched Bending (SENB) specimens following ASTM D5045. Specimens measured $44\times10\times5\,mm^3$, with a notch length of 5 mm and a support span of 40 mm. Quasi-static tests were conducted in three-point bending using the Instron testing machine at a crosshead speed of 10 mm/min, while impact fracture tests were carried out on a CEAST Charpy impact machine in accordance with ISO 17281. A striker mass of 0.5 kg, an initial pendulum angle of 40°, and an impact velocity of 1 m/s were adopted. For both testing conditions, the load–displacement response was recorded at a sampling rate of 500 kHz, without smoothing. At least six specimens were analyzed for every formulation. The critical stress intensity factor, K_{IC}, in Equation (2) was determined from the maximum load according to ASTM D5045,

$$K_{IC} = \frac{P_{max}}{B\sqrt{W}} \cdot f(x) \tag{2}$$

where P_{max} is the maximum load sustained by the samples, B and W are respectively the thickness and the width of the specimen and f(x) is a value provided in the standard as a function of (x=a/W), where a is the notch length. Notably, in the case of impact fracture tests, the maximum load was identified from the load–displacement curves as the maximum relevant load, excluding subsequent oscillations. Moreover, the dynamic loading conditions may introduce inertial and oscillatory effects that are not present in quasi-static testing. Therefore, the calculated value was interpreted as a dynamic fracture toughness. For quasi-static tests, the critical strain energy release rate, G_{IC}, was additionally calculated by integrating the load–displacement curves and evaluating the system compliance, according to the expression reported in Equation (3),

$$G_{IC} = \frac{\Delta U}{BW\varphi} \tag{3}$$

where ΔU is the difference of the total energy absorbed by the sample and the energy absorbed in the indentation tests, and φ is a value reported in the standard as a function of x=a/W.

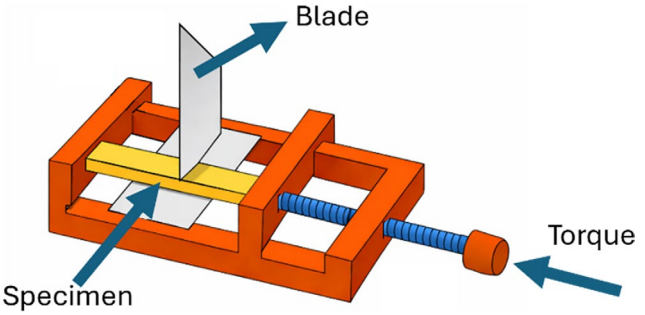


FIGURE 1 | Schematic representation of the device used for the thermal healing process.

2.3.5 | Evaluation of the Self-Healing Efficiency

After fracture testing, the two halves of each SENB specimen (at least six for each composition) were carefully repositioned inside a steel clamping fixture (Figure 1) and compressed under a pressure of 0.5 MPa. The specimens were then thermally treated in an oven at 140°C for 60 min. The healing conditions were selected on the basis of preliminary optimization tests and previous work carried out by our research group [17, 41]. The chosen temperature exceeds the melting temperature of PBS, ensuring sufficient mobility of the molten healing phase and promoting its diffusion into the damaged region.

After thermal treatment, the repaired specimens were re-tested under the same loading configuration (quasi-static or impact) adopted before healing. Damage specimens that failed during handling or healing were excluded. The fracture toughness of the repaired specimens ($K_{IC,H}$) was measured and the healing efficiency (HE) was calculated as the ratio of group-average toughness values, as reported in Equation (4).

$$HE = \frac{K_{IC,H}}{K_{IC}} \tag{4}$$

3 | Results and Discussion

3.1 | Rheological Measurements

In Figure 2a–c, the results obtained from the dynamic rheological measurements on the prepared blends in terms of storage modulus (G'), loss modulus (G''), and magnitude of complex viscosity (η^*) are respectively reported.

The dynamic rheological properties of the blends highlight the significant influence of PBS on the viscoelastic behavior of the materials in the molten state. The incorporation of PBS leads to an increase in G' up to a concentration of 30%vol, suggesting that PBS is likely dispersed as fine domains within the PA6 matrix. This morphology may alter the relaxation dynamic of the PA6 phase and contribute to the more pronounced elastic response. However, at higher PBS contents (40 and 50%vol), G' decreases approaching values comparable to neat PA6, probably because of a progressive PBS phase coalescence. A similar behavior was already observed in a previous work by our group [27], where PBAT dispersed in PLA matrix as small domains increased G′ up to a PBAT content of 10%wt. However, as the amount of PBAT further increased, G' slightly decreased due

15482634, 2026, 11, Downloaded from https://4spepublications.onlinelibrary.wiley.com/doi/10.1002/pen.70863 by Alessandro Pegoretti - Universita Di Trento , Wiley Online Library on [01/11/2025]. See the Terms and Conditions (https://onlinelibrary.wiley.com/terms-and-conditions) on Wiley Online Library for rules of use; OA articles are governed by the applicable Creative Commons License

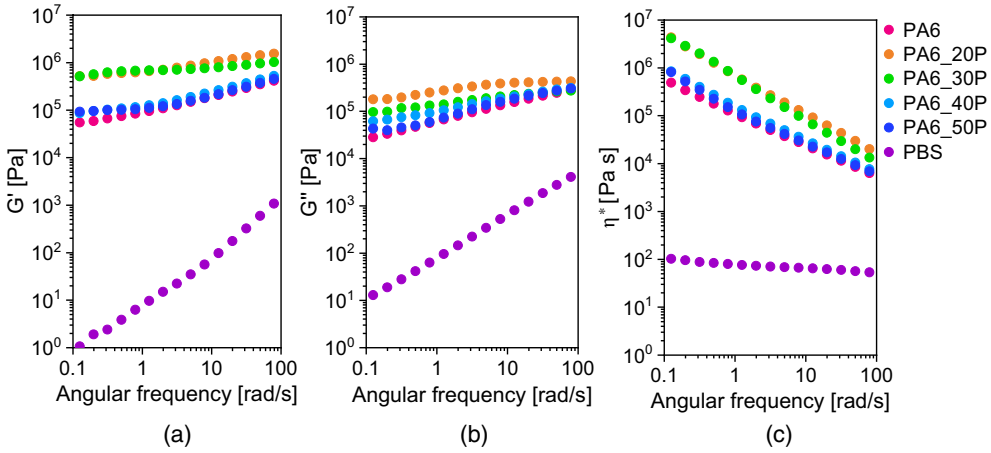


FIGURE 2 | Dynamic rheological behavior of the produced blends ($T = 230°C$). Trends of (a) storage modulus, (b) loss modulus, and (c) magnitude of complex viscosity as a function of the angular frequency.

to PBAT domains coalescence, since the viscoelastic properties (G', G'', η^*) of PBAT were inherently lower than those of PLA. Boonprasertpoh et al. [42] also observed that the viscoelastic properties of PBS/PBAT and PBS/polycaprolactone (PCL) blends first increased with increasing PBAT or PCL content, and then decreased at higher loadings. In that paper, this was associated with a transition from a droplet-like structure to a co-continuous structure. Furthermore, in all the formulated PA6/PBS blends, the comparison between the storage and loss moduli shows that G' remains higher than G'' over the entire frequency range, implying that a predominantly solid-like viscoelastic behavior prevails over a liquid-like one. All formulations exhibit pronounced shear-thinning behavior, as evidenced by the decrease in magnitude of complex viscosity (η^*) with increasing frequency. Neat PA6 displays a complex viscosity approximately 3–4 orders of magnitude higher than that of PBS, indicating that PBS possesses significantly greater melt fluidity and can therefore easily flow within the PA6 matrix during processing or healing. Interestingly, the viscosity of PA6 is enhanced by the introduction of PBS at concentration of 20 and 30%vol, suggesting once again enhanced melt elasticity and good interfacial interaction between the constituents [27]. Conversely, a further increase in the PBS content to 40 and 50%vol results in a decrease in viscosity, approaching values comparable to neat PA6. Overall, the melt viscosity values of all blends remain within a suitable range to ensure efficient processability under standard melt-processing conditions.

3.2 | Chemical and Microstructural Characterization

In Figure 3, the FT-IR spectra of the neat matrices and of the prepared blends are shown.

Neat PA6 exhibits a characteristic N–H stretching vibration at 3292 cm^{-1}, along with the asymmetric and symmetric stretching vibrations of the $-CH_2-$ groups at 2934 and 2853 cm^{-1}, respectively [43]. In addition, the absorption bands at 1637 and 1535 cm^{-1} are assigned to the C=O stretching vibration of amide I and to the combined N–H bending and C–N stretching vibration

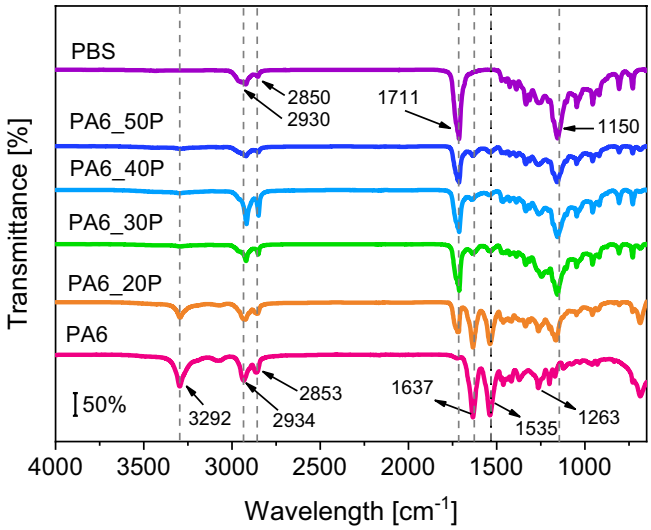


FIGURE 3 | FT-IR spectra of neat PA6, neat PBS, and of the prepared blends.

of amide II, respectively [44]. The peak at 1263 cm^{-1} corresponds to amide III, associated with coupled C–N stretching and N–H bending modes [45]. In contrast, the PBS spectrum shows the characteristic asymmetric and symmetric stretching vibrations of the $-CH_2-$ groups at approximately 2930 and 2850 cm^{-1}, respectively, a strong ester carbonyl (C=O) stretching band at 1711 cm^{-1}, and the stretching vibration of the –C–O–C– group in the ester bonds at around 1150 cm^{-1} [46]. The FTIR spectra of the PA6/PBS blends display no additional bands beyond those of neat PA6 and PBS, nor do they show significant peak shifts. This suggests the absence of strong specific interactions or chemical reactions between the two polymers, supporting the hypothesis that the PA6/PBS system is incompatible. Furthermore, the characteristic peaks of PA6 progressively decrease in intensity with the PBS content, while the PBS bands become more pronounced and visible, reflecting the higher concentration of the PBS phase in the blends.

Figure 4a–f show the FESEM micrographs of the cryofractured surfaces of the prepared formulations, while Figure 4g shows a

15482634, 2026, 11, Downloaded from https://4spepublications.onlinelibrary.wiley.com/doi/10.1002/pen.70863 by Alessandro Pegoretti - Universita Di Trento , Wiley Online Library on [01/11/2025]. See the Terms and Conditions (https://onlinelibrary.wiley.com/terms-and-conditions) on Wiley Online Library for rules of use; OA articles are governed by the applicable Creative Commons License

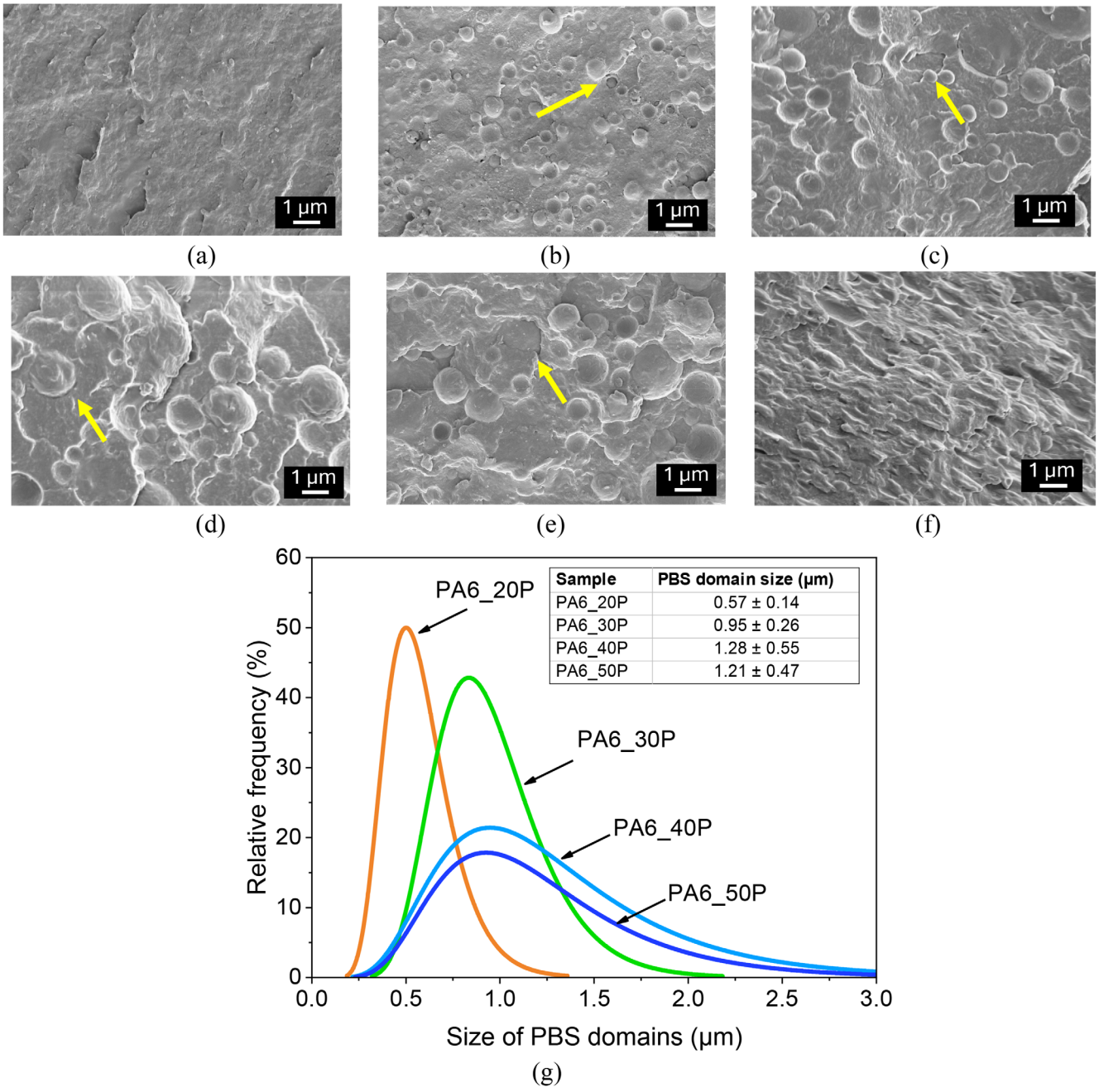


FIGURE 4 | FESEM micrographs of the neat polymers and of the relative blends. (a) PA6, (b) PA6_20P, (c) PA6_30P, (d) PA6_40P, (e) PA6_50P, (f) PBS, (g) log-normal distribution of PBS domains size. The yellow arrows highlight the presence of interfacial debonding between PBS droplets and the PA6 matrix.

quantitative log-normal analysis of the PBS domain size within the blends.

Neat PA6 (Figure 4a) exhibits a relatively smooth fracture surface, whereas PBS shows a more ductile fracture morphology (Figure 4f), consistent with its higher ductility. Figure 4b–e illustrate the typical morphology of incompatible polymer blends, with PBS forming spherical domains dispersed within the continuous PA6 matrix. These domains exhibit a rather good interfacial adhesion with PA6, as there is no significant interfacial debonding or void formation. However, in a few isolated cases, partial detachment at the interface can be detected (highlighted by the yellow arrows in the micrographs). As the PBS content increases from 20 to 50%vol, a progressive evolution in droplet size can be observed. The size distribution of PBS domains (Figure 4g) follows a log-normal behavior for all the investigated blends, indicating a heterogeneous droplet morphology typical of incompatible polymers. The distributions progressively shift toward larger domain sizes and broaden with increasing PBS content, suggesting an evolution toward larger and more heterogeneous PBS domains, which may be associated with increased domain coalescence at higher PBS concentrations. In particular, PA6_20P exhibits the narrowest distribution, with a sharp peak centered at around 0.5–0.6 μm. This indicates a fine and relatively uniform dispersion of small PBS droplets. By increasing the PBS content to 30%vol (PA6_30P), the peak of the distribution

15482634, 2026, 11, Downloaded from https://4spepublications.onlinelibrary.wiley.com/doi/10.1002/pen.70863 by Alessandro Pegoretti - Universita Di Trento , Wiley Online Library on [01/11/2025]. See the Terms and Conditions (https://onlinelibrary.wiley.com/terms-and-conditions) on Wiley Online Library for rules of use; OA articles are governed by the applicable Creative Commons License

shifts to higher values, with the maximum frequency occurring around 0.8–1.0 μm, together with a slightly broader size distribution, reflecting thus the onset of droplet growth and wider size heterogeneity. For PA6_40P and PA6_50P blends, the distributions become significantly broader and flatter, with mean domain size at about 1.20–1.30 μm. The peak frequency decreases while the probability of larger domains increases, consistent with a greater degree of domain aggregation and/or coalescence reaching mean diameter up to 3 μm. This progressive increase in the average size and statistical dispersion of the PBS domains highlights the reduced ability of the PA6 matrix to stabilize the dispersed phase at higher concentrations, resulting in less homogeneous morphologies. It is worth noting that the droplets observed in the micrographs of PA6_50P blend are associated with the PBS phase. This interpretation is supported by the rheological results, since the viscoelastic response (G', G'' and η^*) of PA6_50P largely overlaps with that of neat PA6.

3.3 | Thermal Characterization

Figure 5a,b shows the DSC thermograms of the prepared blends collected during the heating scans (the cooling stage was not shown for brevity), while the most important results are summarized in Table 2.

In the first heating scan, neat PA6 exhibits a melting temperature of 224°C and a rather weak glass transition temperature

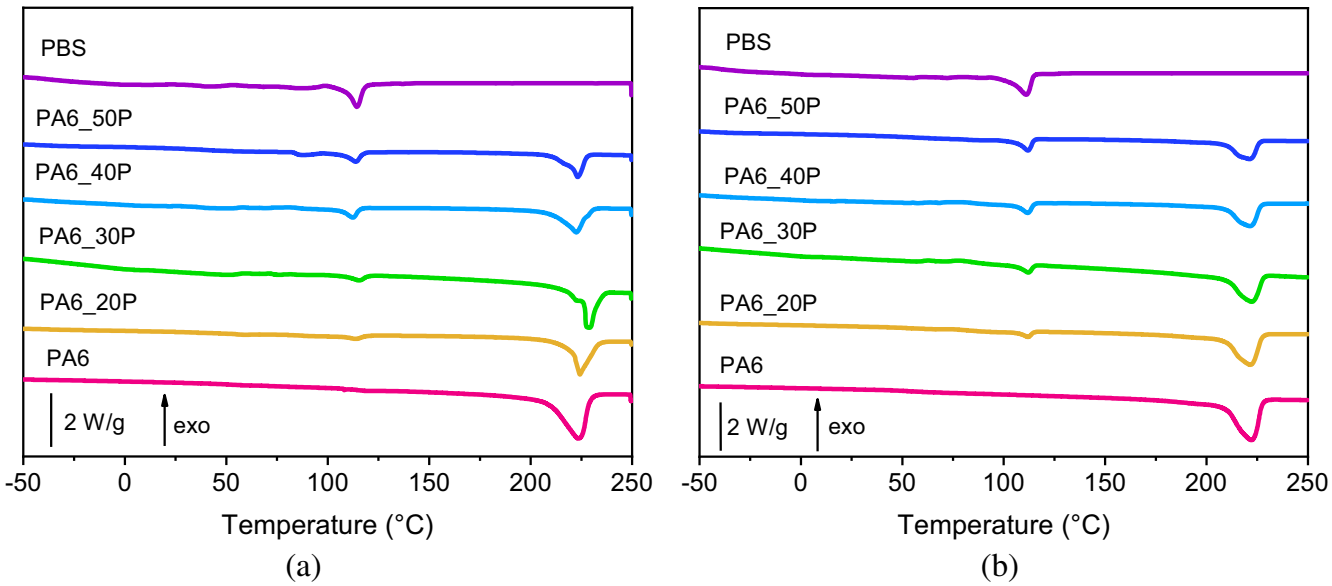


FIGURE 5 | DSC thermograms of the produced blends: (a) first heating scan and (b) second heating scan.

TABLE 2 | Results of the DSC tests on the prepared blends.

Samples	$T_{m,PA6}$ (°C)	$T_{m,PBS}$ (°C)	$\Delta H_{m,PA6}$ (J/g)	$\Delta H_{m,PBS}$ (J/g)	χ_{PA6} (%)	χ_{PBS} (%)
First heating						
PA6	223.5	—	66.5	—	28.9	—
PA6_20P	224.3	114.0	33.8	2.8	18.7	12.1
PA6_30P	228.6	115.4	32.3	3.3	20.6	9.3
PA6_40P	222.5	112.4	31.8	7.4	23.8	16.0
PA6_50P	223.1	107.1	20.9	7.1	19.0	12.4
PBS	—	108.7	—	15.8	—	14.3
Second heating						
PA6	222.1	—	66.3	—	28.8	—
PA6_20P	221.6	111.9	50.3	3.0	27.7	13.0
PA6_30P	222.2	112.1	40.4	8.8	25.8	24.9
PA6_40P	221.6	111.7	38.6	11.6	28.9	25.0
PA6_50P	221.3	112.0	29.1	8.6	26.4	15.0
PBS	—	111.1	—	17.5	—	15.9

15482634, 2026, 11, Downloaded from https://4spepublications.onlinelibrary.wiley.com/doi/10.1002/pen.70863 by Alessandro Pegoretti - Universita Di Trento , Wiley Online Library on [01/11/2026]. See the Terms and Conditions (https://onlinelibrary.wiley.com/terms-and-conditions) on Wiley Online Library for rules of use; OA articles are governed by the applicable Creative Commons License

(T_g) signal at around 60°C, with a PA6 degree of crystallinity of approximately 29%. Similar values were detected by Perin et al. [31] on the same PA6 matrix. In contrast, PBS shows a melting temperature of 109°C and a glass transition at about −38°C (even in this case the T_g signal is barely detectable). The crystallinity of neat PBS is estimated to be around 14%, a value that is in agreement with literature [47]. The progressive incorporation of PBS does not induce significant variations in the melting temperature of PA6, further supporting the incompatibility of the PA6/PBS system. Nevertheless, the addition of PBS slightly reduces the crystallinity of the PA6 phase, which passes from 29% for neat PA6 to about 19% at a PBS content of 50%vol. This progressive reduction may be attributed to the presence of dispersed PBS domains, which can hinder the crystallization of PA6 by limiting its chain mobility. A similar observation was reported by Heidari et al. [48] on PLA/PBAT blends. They found that the presence of PBAT domains with good interfacial adhesion restricted the mobility of the PLA matrix chains, thereby slightly hindering crystal formation. In the second heating scan, the melting temperatures of both PA6 and PBS remain comparable to those observed in the first scan. The crystallinity of PA6 and PBS are overall slightly higher than in the first heating, likely due to the elimination of previous thermal history and to more uniform crystallization during the DSC cooling stage [31]. Overall, DSC results indicate that the incorporation of PBS does not significantly alter the main thermal transitions of the PA6 matrix, confirming the incompatible nature of the prepared blends and suggesting limited interaction between the two polymer phases.

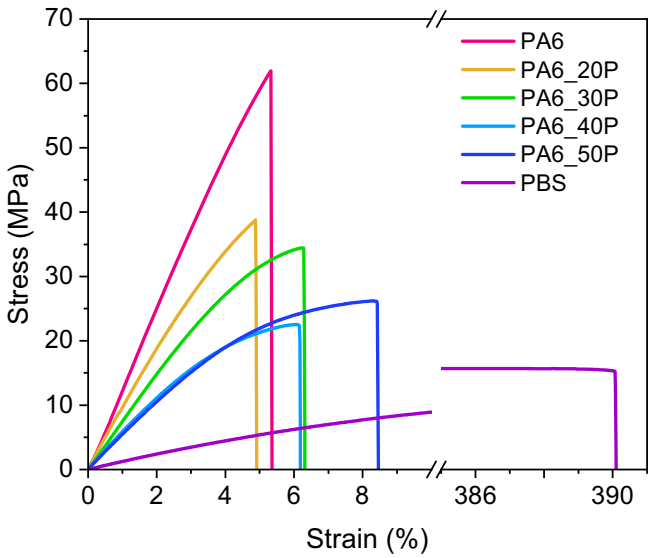


FIGURE 6 | Representative nominal stress–strain curves from quasi-static tensile tests on the prepared blends.

3.4 | Mechanical Characterization

Figure 6 shows representative nominal stress–strain curves from the tensile tests performed on the prepared blends, while Table 3 summarizes the main results collected in tensile and Vicat tests.

Neat PA6 exhibits an elastic modulus of 3.7 GPa, a tensile strength of 57 MPa and an elongation at break of 5%, values that are in good agreement with those reported in the literature for this matrix [31]. In contrast, neat PBS shows a much lower stiffness, with an elastic modulus of 0.2 GPa and a tensile strength of 16 MPa, while displaying a markedly higher ductility, as indicated by an elongation at break of 364%, also consistent with literature data [49]. The incorporation of PBS into the PA6 matrix generally results in a reduction in both elastic modulus and tensile strength, reflecting the softer and ductile character of the PBS phase, and also the incompatible nature of these blends. For instance, the addition of 30%vol of PBS leads to a decrease in modulus of approximately 41% and a reduction in UTS of about 38%, while the elongation at break increases by 24%. However, this increase in strain at failure is not statistically significant compared with neat PA6. A statistically meaningful improvement in elongation at break is only observed at a PBS content of 50%vol, where the strain at failure increases of approximately 61% with respect to neat PA6, indicating a pronounced ductility enhancement at higher PBS fractions. Notably, PA6_40P formulation shows the stronger drop in mechanical performance, with a decrease of 67% in elastic modulus and 60% in tensile strength relative to neat PA6. In view of the possible application of these blends as matrices for self-healing composite laminates, a PBS content of 20–30%vol has been found to provide an acceptable drop of strength and stiffness (compared to neat PA6), while higher PBS loadings result in a excessive reduction in both the modulus and the ultimate tensile strength values. About VST values, PA6 exhibits the highest VST (i.e., 196.1°C), indicating

TABLE 3 | Quasi-static tensile properties and VST of the prepared blend formulations.

Samples	*E* (GPa)	UTS (MPa)	ε_b (%)	VST (°C)
PA6	3.7 ± 0.2^a	56.8 ± 10.4^a	5.1 ± 1.1^a	196 ± 1^a
PA6_20P	2.8 ± 0.2^b	38.6 ± 3.0^b	4.9 ± 0.5^a	191 ± 4^a
PA6_30P	2.2 ± 0.3^c	35.1 ± 2.4^b	6.3 ± 1.2^a	175 ± 5^b
PA6_40P	1.2 ± 0.2^d	22.5 ± 1.6^c	5.9 ± 1.0^a	123 ± 8^c
PA6_50P	1.4 ± 0.1^d	26.5 ± 1.3^c	8.2 ± 0.9^b	104 ± 7^d
PBS	0.2 ± 0.1^e	16.3 ± 0.7^d	363.5 ± 37.6^c	69 ± 2^e

Note: Data are reported as mean ± standard deviation, the statistical significance of these results was assessed by one-way analysis of variance (ANOVA) followed by Tukey's honestly significant difference (HSD) post hoc test ($\alpha = 0.05$). The different superscript letters denote statistically significant differences among groups ($p < 0.05$).

15482634, 2026, 11, Downloaded from https://4spepublications.onlinelibrary.wiley.com/doi/10.1002/pen.70863 by Alessandro Pegoretti - Universita Di Trento , Wiley Online Library on [01/11/2025]. See the Terms and Conditions (https://onlinelibrary.wiley.com/terms-and-conditions) on Wiley Online Library for rules of use; OA articles are governed by the applicable Creative Commons License

TABLE 4 | Critical stress intensity factor (K_{IC}) and critical strain energy release rate (G_{IC}) of neat PA6 and the PA6_30P blend, measured in quasi-static and impact mode.

	Quasi-static mode		Impact mode
Samples	K_{IC} (MPa · $\sqrt{m}$)	G_{IC} (kJ/m^2)	K_{IC} (MPa · $\sqrt{m}$)
PA6	1.20 ± 0.23[a]	0.94 ± 0.46[a]	0.69 ± 0.07[a]
PA6_30P	1.33 ± 0.30[a]	2.07 ± 0.60[b]	1.05 ± 0.22[b]

Note: Data are reported as mean ± standard deviation, the statistical significance of these results was assessed by one-way analysis of variance (ANOVA) followed by Tukey's honestly significant difference (HSD) post hoc test ($\alpha = 0.05$). The different superscript letters denote statistically significant differences among groups ($p < 0.05$).

an optimal dimensional stability, while PBS has a VST of 69°C, due to its intrinsically lower T_m and stiffness [50, 51]. Consequently, the VST progressively decreases with the PBS amount in the blends. For example, by introducing 30%vol of PBS, the VST value is decreased to 175°C and by introducing 50%vol of PBS it further drops down to 104°C. Nevertheless, the VST values remain relatively high up to a PBS content of 30%vol, highlighting that this formulation still retains suitable thermo-mechanical stability for being utilized as matrices of structural composites.

Based on these preliminary morphological and thermo-mechanical screenings, formulations containing 20–30%vol PBS were identified as the range retaining a relatively favorable level of structural performance compared with neat PA6. Since increasing the amount of PBS was expected to increase the fraction of the potential healing phase, PA6_30P was selected as a candidate composition for further evaluation of fracture toughness and self-healing capability. The results reported in Table 4 describe the fracture behavior of neat PA6 and the PA6_30P blend, tested both in quasi-static and impact mode, in terms of their K_{IC} and G_{IC} values.

In quasi-static mode, neat PA6 exhibits a fracture toughness K_{IC} of 1.20 MPa$\sqrt{m}$ and a critical strain energy release rate G_{IC} of 0.94 kJ/m^2, these values are rather lower than those commonly reported in the literature for polyamide 6 (i.e., approximately 2–3 MPa$\sqrt{m}$ for K_{IC} and 3–5 kJ/m^2 for G_{IC} [52]). However, it is important to note that the fracture toughness of thermoplastic polymers such as PA6 is highly sensitive to various factors, particularly the processing conditions, moisture content, pre-cracking procedure and notch geometry. Indeed, processing conditions can strongly influence the fracture toughness of polymers by modifying their crystallinity, defect content and energy dissipation mechanisms during crack propagation [53]. Furthermore, moisture acts as a plasticizer and can significantly increase ductility and toughness, whereas dry specimens tend to fail in a more brittle way [54, 55]. Finally, notch geometry and pre-cracking procedures can markedly affect the K_{IC} value, since crack initiation in polymers is highly sensitive to stress concentration at the crack tip [56]. The value obtained in this work is therefore consistent with the expected variability of PA6 fracture toughness and provides a suitable baseline for the evaluation of the toughening and self-healing contributions introduced by PBS in the blends. Indeed, the incorporation of PBS leads to a slight increase in K_{IC} compared to neat PA6 (approximately 11%), though this difference is not statistically significant. This limited improvement may be attributed to the toughening effect provided by PBS, as well as to the rather good interfacial adhesion between PA6 and PBS domains, that limits debonding events. A particularly important effect due to PBS incorporation is observed in terms of the strain energy release rate (G_{IC}). While the increase in K_{IC} is relatively modest, G_{IC} shows a remarkable improvement upon PBS addition. Specifically, it increases of about 120% with respect to neat PA6 and indicates that the blend is able to dissipate significantly more energy during crack propagation than the neat PA6 matrix. Under impact loading, the dynamic fracture toughness of neat PA6 is 0.69 MPa$\sqrt{m}$, that is, lower than that measured in quasi-static mode. This reduction is attributed to the higher deformation rate that could have altered the viscoelastic response of the material, resulting in lower peak loads during testing. Such behavior highlights that different mechanisms govern crack initiation and propagation under quasi-static and impact conditions [31]. The incorporation of PBS leads to a significant increase in the dynamic fracture toughness value compared to neat PA6 (approximately 52%), even higher than that previously observed in quasi-static mode. Overall, the presence of PBS has a beneficial effect on the fracture toughness (and dynamic fracture toughness) of PA6, enhancing its resistance to crack propagation under both loading regimes. These findings are further supported by FESEM micrographs of the fracture surfaces of SENB specimens after testing, shown in Figure 7.

The fracture morphology differs markedly between the specimens tested in quasi-static and impact conditions. In quasi-static mode, both neat PA6 and the PA6_30P blend display pronounced plastic deformation, with the fracture surface appearing particularly irregular. Conversely, specimens tested under impact conditions exhibit much smoother fracture surfaces, with no evidence of plastic deformation in the neat PA6 and only limited deformation in PA6_30P. A smoother crack surface may facilitate the healing process by enabling the healing phase to spread more uniformly across the fracture plane, whereas a rough and highly deformed surface may hinder diffusion and wetting. Notably, PBS domains are clearly visible within the deformed PA6 matrix in both quasi-static and impact blends, confirming their involvement in the fracture process.

3.5 | Evaluation of the Self-Healing Efficiency

Table 5 summarizes the fracture toughness values of the healed specimens ($K_{IC,H}$), alongside the corresponding self-healing efficiency (HE) values, measured under quasi-static and impact mode.

15482634, 2026, 11, Downloaded from https://4spepublications.onlinelibrary.wiley.com/doi/10.1002/pen.70863 by Alessandro Pegoretti - Universita Di Trento , Wiley Online Library on [01/11/2025]. See the Terms and Conditions (https://onlinelibrary.wiley.com/terms-and-conditions) on Wiley Online Library for rules of use; OA articles are governed by the applicable Creative Commons License

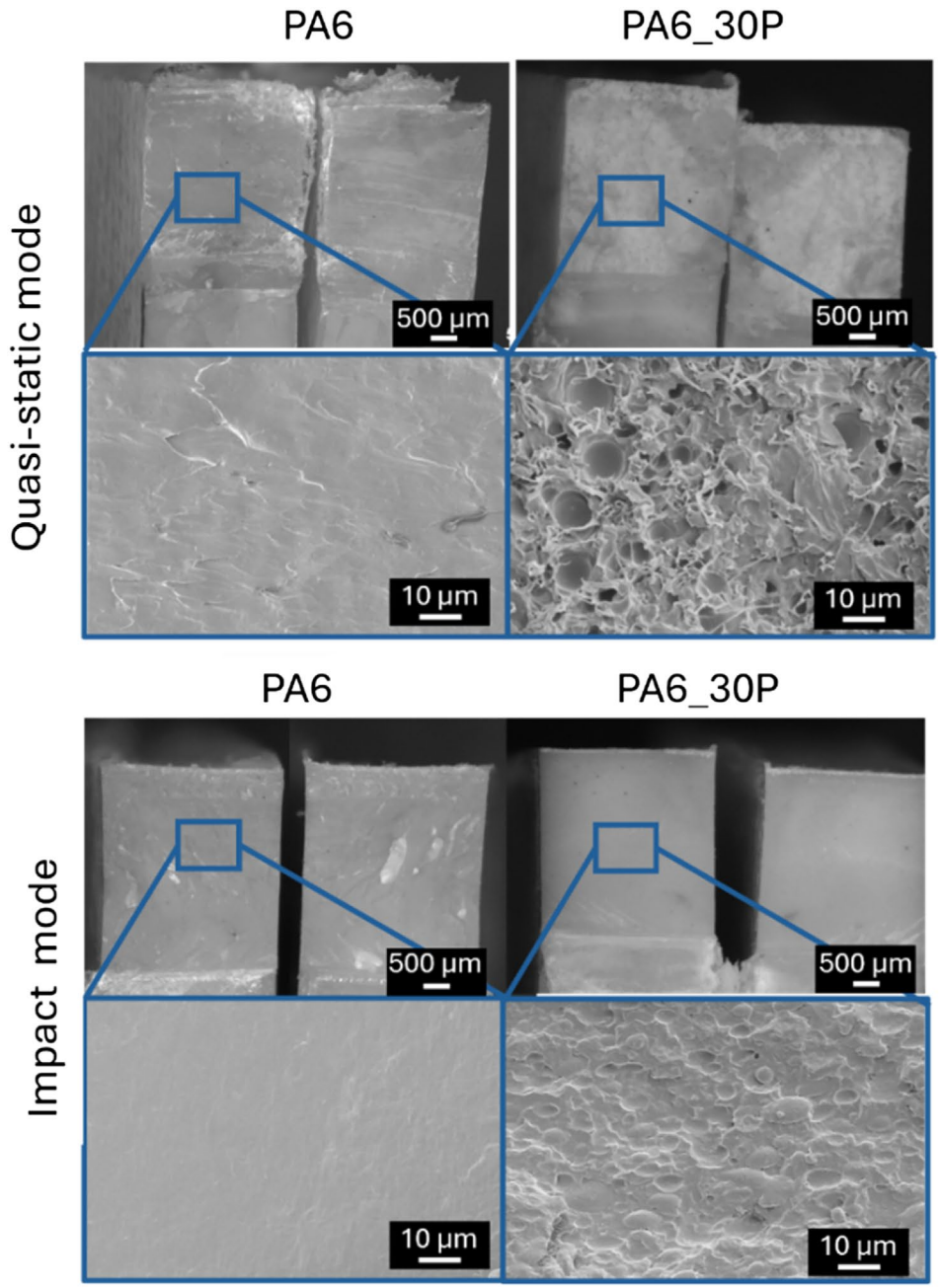


FIGURE 7 | FESEM micrographs of the fracture surface of the SENB specimens tested in quasi-static and impact mode.

TABLE 5 | Critical stress intensity factor of healed blends ($K_{IC,H}$) and healing efficiency values (HE) of neat PA6 and PA6_30P blend tested in quasi-static and impact mode.

	Quasi-static mode		Impact mode	
Samples	$K_{IC,H}$ **(MPa** $\cdot \sqrt{m}$**)**	**HE (%)**	$K_{IC,H}$ **(MPa** $\cdot \sqrt{m}$**)**	**HE (%)**
PA6	—	—	—	—
PA6_30P	0.23 ± 0.05	17.3 ± 5.4[a]	0.42 ± 0.18	40.0 ± 19.1[a]

Note: Data are reported as mean ± standard deviation, the statistical significance of these results was assessed by one-way analysis of variance (ANOVA) followed by Tukey's honestly significant difference (HSD) post hoc test ($\alpha = 0.05$). The different superscript letters denote statistically significant differences among groups ($p < 0.05$).

The analysis of the fracture toughness values ($K_{IC,H}$) of the healed specimens demonstrates that the presence of PBS in the fracture area is essential to achieve fracture toughness recovery. Neat PA6 shows no measurable recovery of K_{IC} and therefore its healing efficiency cannot be defined. In contrast, the addition of PBS results in a clear change in

15482634, 2026, 11, Downloaded from https://4spepublications.onlinelibrary.wiley.com/doi/10.1002/pen.70863 by Alessandro Pegoretti - Universita Di Trento , Wiley Online Library on [01/11/2025]. See the Terms and Conditions (https://onlinelibrary.wiley.com/terms-and-conditions) on Wiley Online Library for rules of use; OA articles are governed by the applicable Creative Commons License

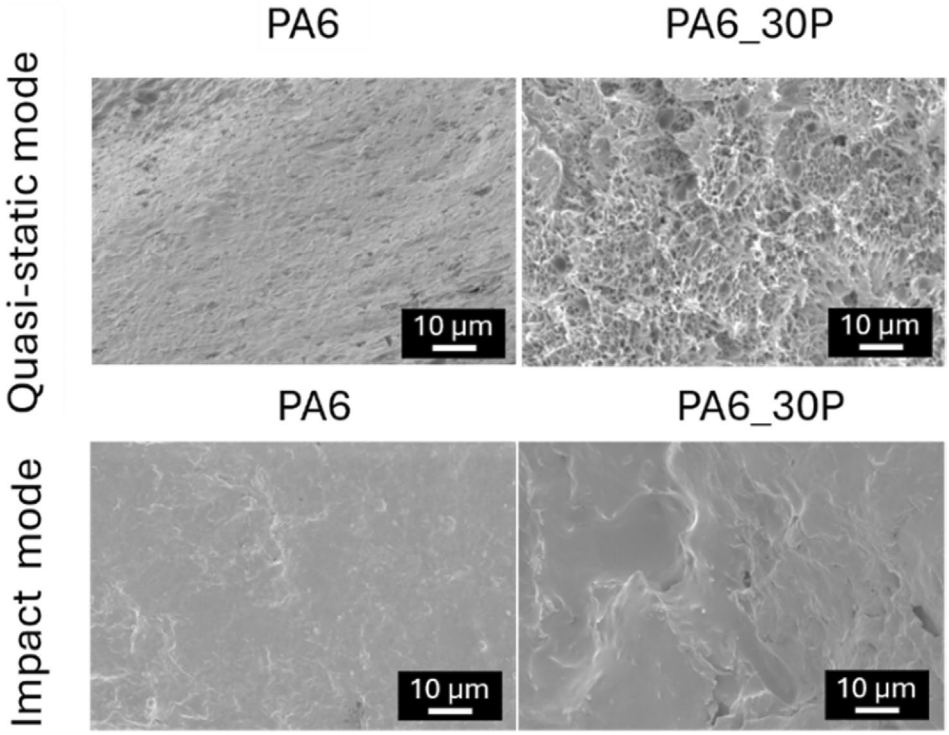


FIGURE 8 | FESEM micrographs of the fracture surface of the healed SENB specimens after testing in quasi-static and impact mode.

healing behavior, leading to measurable fracture toughness restoration, reaching 17.3% in quasi-static mode and 40% under impact conditions. The enhanced repair performance under impact loading is likely associated with the higher strain rate, which produces smoother and less plastically deformed fracture surfaces (see Figure 7). This morphology promotes PBS flow and spreading along the crack plane. In contrast, the application of a quasi-static loading generates highly irregular and plastically deformed surfaces, which restrict PBS diffusion into the damaged region and limits crack closure. FESEM micrographs of the fracture surfaces after the healing process, reported in Figure 8, further corroborate these considerations.

Regardless of the testing speed, the fracture surface of neat PA6 remains essentially unchanged after healing. By contrast, PA6_30P exhibits a markedly smoother morphology after the healing treatment, with the PBS domains appearing less clearly distinguishable and a more continuous phase being observed along portions of the fracture surface. Considering that the healing treatment was performed at 140°C, that is above the melting temperature of PBS, this morphological evolution is consistent with an hypothetical partial melting and redistribution of the PBS phase across the damaged interface. In quasi-static conditions, however, the fracture surfaces remain irregular and plastically deformed, possibly limiting an uniform PBS flow and preventing complete wetting of the damaged areas. Conversely, under impact loading, the smoother and more regular fracture morphology may favors a more homogeneous distribution of the PBS film, that could explain the higher healing efficiencies observed in impact loading. This behavior was already observed by Perin et al. [31, 36, 37], where smoother and more regular fracture morphologies detected in PA6/COC and PA6/PCL blends under impact loading led to higher self-healing efficiencies (35%–60%) than those recorded under quasi-static conditions (5%–30%).

It can be concluded that PBS can be successfully incorporated into the PA6 matrix to enhance its fracture toughness and to impart self-healing capability. In future work, the introduction of a compatibilizer, such as an epoxy-based chain extender, could represent a promising strategy to further enhance the strength, stiffness, and fracture toughness of this blend. Indeed, the compatibilization may promote chemical interactions between the functional epoxy groups and the end groups of PA6 and PBS, leading to improved interfacial adhesion between the dispersed PBS domains and the surrounding PA6 matrix. This enhanced compatibility could also suppress droplet coalescence, refine the phase morphology, and thus promote more efficient stress transfer across the interface, ultimately resulting in improved mechanical and fracture performance. For this reason, a compatibilized PA6_30P composition will be further explored in the future for the development of composite laminates with intrinsic self-healing functionality. Moreover, the healing efficiency should also be evaluated after multiple repair cycles in order to assess the repeatability of the self-healing effect.

4 | Conclusions

In this work, polyamide 6/poly(butylene succinate) (PA6/PBS) blends were developed and systematically characterized to assess their suitability as self-healing matrices for structural thermoplastic composites. Blends containing 20–50%vol PBS were prepared by melt compounding and hot pressing.

15482634, 2026, 11, Downloaded from https://4spepublications.onlinelibrary.wiley.com/doi/10.1002/pen.70863 by Alessandro Pegoretti - Universita Di Trento , Wiley Online Library on [01/11/2025]. See the Terms and Conditions (https://onlinelibrary.wiley.com/terms-and-conditions) on Wiley Online Library for rules of use; OA articles are governed by the applicable Creative Commons License

Their rheological, morphological, thermal, and mechanical behavior was comprehensively investigated, with particular emphasis on fracture toughness and thermally activated self-healing. Rheological analyses revealed that the incorporation of lower PBS contents increased the storage modulus (G'), loss modulus (G''), and magnitude of complex viscosity (η), while maintaining melt processability compatible with conventional processing techniques. FESEM observations confirmed the formation of an incompatible morphology, consisting of well-dispersed PBS domains embedded within the PA6 matrix, with satisfactory interfacial adhesion up to a PBS content of 30%vol. The progressive addition of PBS reduced the tensile stiffness and strength of PA6 owing to the lower mechanical properties of the dispersed phase. The PA6/PBS blend containing 30%vol PBS was selected as a candidate composition for detailed fracture toughness and self-healing characterization based on the preliminary thermo-mechanical screening. This formulation retained a relatively high level of stiffness, strength, and thermal stability compared with the formulation containing higher PBS concentrations, while potentially providing a higher fraction of the healing phase than PA6_20P. Under the adopted healing conditions, PA6_30P exhibited measurable recovery of fracture toughness, reaching approximately 17% under quasi-static loading and 40% under impact loading conditions, whereas neat PA6 showed no measurable healing. The higher healing efficiency observed under impact loading was attributed to the smoother fracture surfaces generated at high strain rates, which could have promoted the melting, flow, and redistribution of the PBS phase along the crack interface. These findings demonstrate the potential of PBS as both a toughening and thermally activated healing phase for PA6. Future work will focus on the development of compatibilized PA6/PBS systems for multifunctional composite laminates and on evaluating the durability of the self-healing mechanism through repeated damage-healing cycles.

Author Contributions

Laura Simonini: conceptualization, methodology, data curation, investigation, validation, formal analysis, visualization, project administration, writing – original draft, writing – review and editing, software. **Riccardo Ramundo:** investigation, formal analysis, methodology, visualization. **Daniele Rigotti:** conceptualization, investigation, formal analysis, writing – review and editing. **Alessandro Sorze:** conceptualization, investigation, formal analysis, writing – review and editing. **Alessandro Pegoretti:** writing – review and editing, supervision. **Andrea Dorigato:** supervision, funding acquisition, writing – review and editing, resources, validation.

Acknowledgments

Open access publishing facilitated by Universita degli Studi di Trento, as part of the Wiley - CRUI-CARE agreement.

Conflicts of Interest

The authors declare no conflicts of interest.

Data Availability Statement

The data that support the findings of this study are available from the corresponding author upon reasonable request.

References

1. J. Tang, Z. Zhou, H. Chen, et al., "Laminate Design, Optimization, and Testing of an Innovative Carbon Fiber-Reinforced Composite Sandwich Panel for High-Speed Train," *Polymer Composites* 42 (2021): 5811–5829.

2. A. Kausar, I. Ahmad, S. Rakha, M. Eisa, and A. Diallo, "State-Of-The-Art of Sandwich Composite Structures: Manufacturing—To—High Performance Applications," *Journal Of Composites Science* 7 (2023): 102–108.

3. L. Simonini, A. Sorze, L. Maddalena, F. Carosio, and A. Dorigato, "Mechanical Reprocessing of Polyurethane and Phenolic Foams to Increase the Sustainability of Thermal Insulation Materials," *Polymer Testing* 138 (2024): 108539.

4. M. Celiński, K. Sałasińska, K. Mizera, and P. Kozikowski, "Fire Behavior of Sandwich Panels With Different Cores," *Advances in the Toxicity of Construction and Building Materials* 1 (2022): 137–170.

5. N. Truschelli, L. Simonini, A. Tempelis, L. Mishnaevsky, Jr., A. Pegoretti, and A. Dorigato, "Development of Self-Healing Epoxy/COC Adhesives for Potential Use in Wind Turbine Blades," *Composites Part A: Applied Science and Manufacturing* 205 (2026): 109732.

6. A. Sorze, F. Valentini, A. Dorigato, and A. Pegoretti, "Salt Leaching as a Green Method for the Production of Polyethylene Foams for Thermal Energy Storage Applications," *Polymer Engineering and Science* 62 (2022): 1650–1663.

7. H. Silu, W. Bo, and Y. Libo, "Interphase and Interfacial Properties of Composite Materials," in *Composite Materials: Manufacturing, Properties and Applications* (Elsevier, 2021), 151–177.

8. P. Romanowic and A. Muc, "Estimation of Notched Composite Plates Fatigue Life Using Residual Strength Model Calibrated by Step-Wise Tests," *Materials* 11 (2018): 2180–2199.

9. L. Simonini, H. Mahmood, A. Dorigato, and P. Alessandro, "Development of a Self-Healing Interphases for Structural Composites," in *Proceedings of the 23rd International Conference on Composite Materials, ICCM 2023* (European Society for Composite Materials (ESCM), 2023).

10. H. Mahmood, L. Simonini, A. Dorigato, and A. Pegoretti, "Graphene Deposition on Glass Fibers by Triboelectrification," *Applied Sciences* 11 (2021): 3123–3135.

11. L. Simonini, H. Mahmood, A. Dorigato, and A. Pegoretti, "Evaluation of Self-Healing Capability of a Polycaprolactone Interphase in Epoxy/Glass Composites," *Composites Part A: Applied Science and Manufacturing* 169 (2023): 107539.

12. L. Simonini, M. Kakkonen, R. Dsouza, et al., "Tailoring the Interfacial Properties of Glass Fiber-Epoxy Microcomposites Through the Development of a Self-Healing Poly (ε-Caprolactone) Coating," *Composites Science and Technology* 261 (2025): 110991.

13. Y. Sun, L. Simonini, C. Xing, and L. Mishnaevsky, Jr., "Self-Healing Interfaces in Fiber Reinforced Polymers: Computational Modeling," *Composites Science and Technology* 270 (2025): 111269.

14. L. Simonini, R. Canale, H. Mahmood, A. Dorigato, and A. Pegoretti, "Multifunctional Epoxy/Carbon Composites With a Fully Reparable Interface," *Polymer Composites* 45 (2024): 2558–2568.

15. L. Simonini and A. Dorigato, "Surface Modification of Wood Fibers With Citric Acid as a Sustainable Approach to Developing Novel Polycaprolactone-Based Composites for Packaging Applications," *Journal Of Composites Science* 9 (2025): 274–289.

16. H. Mahmood, A. Dorigato, and A. Pegoretti, "Healable Carbon Fiber-Reinforced Epoxy/Cyclic Olefin Copolymer Composites," *Materials* 13 (2020): 2165.

17. R. C. Zovi, H. Mahmood, A. Dorigato, G. Fredi, and A. Pegoretti, "Cyclic Olefin Copolymer Interleaves for Thermally Mendable Carbon/Epoxy Laminates," *Molecules* 25 (2020): 5347.

15482634, 2026, 11, Downloaded from https://4spepublications.onlinelibrary.wiley.com/doi/10.1002/pen.70863 by Alessandro Pegoretti - Universita Di Trento , Wiley Online Library on [01/11/2025]. See the Terms and Conditions (https://onlinelibrary.wiley.com/terms-and-conditions) on Wiley Online Library for rules of use; OA articles are governed by the applicable Creative Commons License

18. A. Cohades, C. Branfoot, S. Rae, I. Bond, and V. Michaud, "Progress in Self-Healing Fiber-Reinforced Polymer Composites," *Advanced Materials Interfaces* 5 (2018): 1800177.

19. R. S. Trask, H. R. Williams, and I. P. Bond, "Self-Healing Polymer Composites: Mimicking Nature to Enhance Performance," *Bioinspiration & Biomimetics* 2 (2007): 1–10.

20. A. R. Jones, B. J. Blaiszik, S. R. White, and N. R. Sottos, "Full Recovery of Fiber/Matrix Interfacial Bond Strength Using a Microencapsulated Solvent-Based Healing System," *Composites Science and Technology* 79 (2013): 1–7.

21. C. J. Norris, G. J. Meadway, M. J. O'Sullivan, I. P. Bond, and R. S. Trask, "Self-Healing Fibre Reinforced Composites via a Bioinspired Vasculature," *Advanced Functional Materials* 21 (2011): 3624–3633.

22. H. Ghazali, L. Ye, and A. N. Amir, "Microencapsulated Healing Agents for an Elevated-Temperature Cured Epoxy: Influence of Viscosity on Healing Efficiency," *Polymers and Polymer Composites* 29 (2021): 1317–1327.

23. W. Zhang, J. Duchet, and J. F. Gerard, "Self-Healable Interfaces Based on Thermo-Reversible Diels–Alder Reactions in Carbon Fiber Reinforced Composites," *Journal of Colloid and Interface Science* 430 (2014): 61–68.

24. H. Zhang, K. Lamnawar, and A. Maazouz, "Rheological Modeling of the Diffusion Process and the Interphase of Symmetrical Bilayers Based on PVDF and PMMA With Varying Molecular Weights," *Rheologica Acta* 51 (2012): 691–711.

25. D. Y. Wu, S. Sam Meure, and D. Solomon, "Self-Healing Polymeric Materials: A Review of Recent Developments," *Progress in Polymer Science* 33 (2008): 479–522.

26. S. Islam and G. Bhat, "Progress and Challenges in Self-Healing Composite Materials," *Materials Advances* 2 (2012): 1896–1926.

27. I. Savioli, L. Simonini, D. Rigotti, A. Pegoretti, and A. Dorigato, "Biodegradable Poly (Lactic Acid)-Based Blends as Intrinsic Self-Healing Matrices for Multifunctional and Eco-Sustainable Composites," *Molecules* 31 (2026): 921–941.

28. M. Peñas-Caballero, M. H. Santana, R. Verdejo, and M. A. Lopez-Manchado, "Polymer Blends as an Effective Strategy to Designing Self-Healing Epoxy Resin," *Composites Part A: Applied Science and Manufacturing* 200 (2025): 109390.

29. GrandViewResearch, "Thermoplastic Composites Market (2022–2030)," (2021), https://www.grandviewresearch.com/industry-analysis/thermoplastic-composites-market-report.

30. M. Kohutiar, L. Kakošová, M. Krbata, et al., "Comprehensive Review: Technological Approaches, Properties, and Applications of Pure and Reinforced Polyamide 6 (PA6) and Polyamide 12 (PA12) Composite Materials," *Polymers* 17, no. 4 (2025): 442.

31. D. Perin, G. Odorizzi, A. Dorigato, and A. Pegoretti, "Development of Polyamide 6 (PA6)/Polycaprolactone (PCL) Thermoplastic Self-Healing Polymer Blends for Multifunctional Structural Composites," *Applied Sciences* 12 (2022): 12357.

32. A. Sorze, F. Valentini, S. Santi, et al., "Assessing Natural Fillers as Substitutes for Glass Fibers in Polyamide 6 Composites for Large-Format Additive Manufacturing," *Polymers* 18 (2026): 1049.

33. A. Sorze, R. Miani, C. Gioia, G. Fredi, and A. Dorigato, "Improved Thermo-Mechanical and Flame Resistance Behaviour of Polyamide 6/Lignin Microcomposites," *Macromolecules* 6 (2026): 18.

34. P. Wang, L. Yang, Y. Zhou, et al., "Synergistic Effect of EVA-GMA and Nanofillers on Mechanical and Dielectric Properties of Polyamide," *Composites Communications* 25 (2021): 100738.

35. M. Y. Kondo, L. S. Montagna, G. F. D. M. Morgado, et al., "Recent Advances in the Use of Polyamide-Based Materials for the Automotive Industry," *Polímeros* 32 (2022): 2022023.

36. D. Perin, A. Dorigato, and A. Pegoretti, "Compatibilization of Polyamide 6/Cyclic Olefinic Copolymer Blends for the Development of Multifunctional Thermoplastic Composites With Self-Healing Capability," *Materials* 17 (2024): 1880–1893.

37. D. Perin, L. Botta, D. Rigotti, D. Dorigato, G. Fredi, and A. Pegoretti, "Tuning the Compatibilizer Content and Healing Temperature in Thermally Mendable Polyamide 6/Cyclic Olefinic Copolymer Blends," *Polymers* 17 (2025): 280–293.

38. V. Rajgond, A. Mohite, N. More, and A. More, "Biodegradable Polyester-Polybutylene Succinate (PBS): A Review," *Polymer Bulletin* 81 (2024): 5703–5752.

39. C. Millot, L. A. Fillot, O. Lame, P. Sotta, and R. Seguela, "Assessment of Polyamide-6 Crystallinity by DSC: Temperature Dependence of the Melting Enthalpy," *Journal of Thermal Analysis and Calorimetry* 122 (2015): 307–314.

40. S. Chen, S. Li, B. Wang, C. Chen, and L. Zheng, "Preparation and Performance of Poly(Butylene Succinate) (PBS) Composites Reinforced With Taxus Residue and Compatibilized With Branched PBS," *Polymers* 17 (2025): 2597–2610.

41. L. Simonini, G. Fuoli, A. Sorze, A. Pegoretti, and A. Dorigato, "Evaluation of the Self-Healing Behaviour of Structural Polyamide 6 (PA6)/Poly (Butylene-Adipate-Terephthalate)(PBAT) Blends," *Journal Of Composites Science* 10 (2026): 435–454.

42. A. Boonprasertpoh, D. Pentrakoon, and J. Junkasem, "Investigating Rheological, Morphological and Mechanical Properties of PBS/PBAT Blends," *Journal Of Metals, Materials and Minerals* 27 (2017): 1–11.

43. D. E. Kherroub, M. Belbachir, S. Lamouri, L. Bouhadjar, and K. Chikh, "Synthesis of Polyamide-6/Montmorillonite Nanocomposites by Direct In-Situ Polymerization Catalysed by Exchanged Clay," *Oriental Journal of Chemistry* 29 (2013): 1429–1436.

44. M.-Y. Lim, H. J. Kim, S. J. Baek, K. Y. Kim, S. S. Lee, and J. C. Lee, "Improved Strength and Toughness of Polyketone Composites Using Extremely Small Amount of Polyamide 6 Grafted Graphene Oxides," *Carbon* 77 (2014): 366–378.

45. B. De Campos Vidal, "Using the FT-IR Linear Dichroism Method for Molecular Order Determination of Tendon Collagen Bundles and Nylon 6," *Acta Histochemica* 115 (2013): 686–691.

46. F. Barrino, H. De La Rosa-Ramírez, C. Schiraldi, J. López-Martínez, and M. D. Samper, "Preparation and Characterization of New Bioplastics Based on Polybutylene Succinate (PBS)," *Polymers* 15 (2023): 1212–1230.

47. M. Bianchi, A. Dorigato, M. Morreale, and A. Pegoretti, "Evaluation of the Physical and Shape Memory Properties of Fully Biodegradable Poly (Lactic Acid)(PLA)/Poly (Butylene Adipate Terephthalate)(PBAT) Blends," *Polymers* 15, no. 4 (2023): 881–897.

48. M. Heidari and H. Garmabi, "Design, Modeling, and Optimization of PLA/PBAT Using Response Surface Method: Rheology and Comprehensive Characterization for 3D Printing Applications," *Materials Today Communications* 50 (2025): 114164.

49. S. A. Rafiqah, A. Khalina, A. S. Harmaen, et al., "A Review on Properties and Application of Bio-Based Poly (Butylene Succinate)," *Polymers* 13 (2021): 1436–1464.

50. S. C. Ozmen, G. Ozkoc, and E. Serhatli, "Thermal, Mechanical and Physical Properties of Chain Extended Recycled Polyamide 6 via Reactive Extrusion: Effect of Chain Extender Types," *Polymer Degradation and Stability* 162 (2019): 76–84.

51. X. Yan, L. Chen, H. Tian, et al., "Enhancement of the Compatibility, Mechanical Properties, and Heat Resistance of Poly (Butylene Succinate-Co-Terephthalate)/Poly (Butylene Succinate) Blends by the Addition of Chain Extender and Nucleating Agent," *Journal of Polymer Research* 30 (2023): 111–123.

52. S. Siengchin and J. Karger-Kocsis, "Structure, Mechanical, and Fracture Properties of Nanoreinforced and HNBR-Toughened Polyamide-6," *Journal of Applied Polymer Science* 123 (2012): 897–902.

15482634, 2026, 11, Downloaded from https://4spepublications.onlinelibrary.wiley.com/doi/10.1002/pen.70863 by Alessandro Pegoretti - Universita Di Trento , Wiley Online Library on [01/11/2026]. See the Terms and Conditions (https://onlinelibrary.wiley.com/terms-and-conditions) on Wiley Online Library for rules of use; OA articles are governed by the applicable Creative Commons License

53. F. T. Ibáñez-Gutiérrez, S. Cicero, and I. A. Carrascal, "On the Influence of Moisture Content on the Fracture Behaviour of Notched Short Glass Fibre Reinforced Polyamide 6," *Composites Part B: Engineering* 159 (2019): 62–71.

54. M. Ahmadifar, K. Benfriha, and M. Shirinbayan, "Thermal, Tensile and Fatigue Behaviors of the PA6, Short Carbon Fiber-Reinforced PA6, and Continuous Glass Fiber-Reinforced PA6 Materials in Fused Filament Fabrication (FFF)," *Polymers* 15 (2023): 507–520.

55. V. S. Balakrishnan, K. Wartig, N. Tsombanis, and H. Seidlitz, "Influence of Processing Parameters on the Impact Behaviour of Glass/Polyamide-6 Composite," *Composites Part B: Engineering* 159 (2019): 292–299.

56. J. M. de Souza, H. N. Yoshimura, F. M. Peres, and C. G. Schön, "Effect of Sample Pre-Cracking Method and Notch Geometry in Plane Strain Fracture Toughness Tests as Applied to a PMMA Resin," *Polymer Testing* 31 (2012): 834–840.

Supporting Information

Additional supporting information can be found online in the Supporting Information section. **Figure S1:** Results of TGA analysis on neat PA6 and neat PBS. Trends of (a) residual mass and (b) derivative of residual mass loss (DTG).

15482634, 2026, 11, Downloaded from https://4spepublications.onlinelibrary.wiley.com/doi/10.1002/pen.70863 by Alessandro Pegoretti - Universita Di Trento , Wiley Online Library on [01/11/2026]. See the Terms and Conditions (https://onlinelibrary.wiley.com/terms-and-conditions) on Wiley Online Library for rules of use; OA articles are governed by the applicable Creative Commons License